




Band gap opening in graphene by hybridization with Au (001) reconstructed surfacesTomo-o Terasawa ^{1,2,*}, Kazuya Matsunaga,³ Naoki Hayashi,³ Takahiro Ito ^{3,4}, Shin-ichiro Tanaka,⁵ Satoshi Yasuda ¹ and Hidehito Asaoka¹¹Advanced Science Research Center, Japan Atomic Energy Agency, 2–4 Shirakata, Tokai, Ibaraki 319–1195, Japan²Institute of Industrial Science, The University of Tokyo, 4-6-1 Komaba, Meguro, Tokyo 153–8505, Japan³Graduate School of Engineering, Nagoya University, Furo-cho, Chikusa, Nagoya 464–8603, Japan⁴Synchrotron radiation Research center, Nagoya University, Furo-cho, Chikusa, Nagoya 464–8603, Japan⁵SANKEN, The Institute of Scientific and Industrial Research, Osaka University, 8-1 Mihogaoka, Ibaraki, Osaka 567–0047, Japan

(Received 29 December 2021; revised 8 October 2022; accepted 6 December 2022; published 11 January 2023)

Au(001) surfaces exhibit a complex reconstructed structure [Hex–Au(001)] comprising a hexagonal surface and square bulk lattices, yielding a quasi-one-dimensional corrugated surface. When graphene was grown on this surface, the periodicity of the corrugated surface was predicted to change the electronic structure of graphene, forming bandgaps and new Dirac points. Furthermore, the graphene–Au interface is promising for bandgap generation and spin injection due to band hybridization. Here, we report the angle-resolved photoemission spectroscopy and density functional calculation of graphene on a Hex–Au(001) surface. The crossing point of the original and replica graphene π bands showed no bandgap, suggesting that the one-dimensional potential was too small to modify the electronic structure. A bandgap of 0.2 eV was observed at the crossing point of the graphene π and Au $6sp$ bands, indicating that the bandgap is generated using hybridization of the graphene π and Au $6sp$ bands. We discussed the hybridization mechanism and concluded that the R30 configuration between graphene and Au and an isolated electronic structure of Au are essential for effective hybridization between graphene and Au. We anticipate that hybridization between graphene π and Au $6sp$ would result in spin injection into graphene.

DOI: [10.1103/PhysRevMaterials.7.014002](https://doi.org/10.1103/PhysRevMaterials.7.014002)**I. INTRODUCTION**

The modification of the band structure of graphene by periodic potentials plays a vital role in both fundamental physics and applications of graphene, as it fascinates properties such as superconductivity in graphene [1–3]. It was expected that using a one-dimensional (1D) periodic potential would make the band structure of graphene anisotropic, with new Dirac points at zone boundaries crossing the potential and high group velocities along the potential [1]. Such an electronic structure is promising for graphene field effect transistor (FET) devices using transport anisotropy and resistance peaks [2,4]. Extensive experimental research has been conducted on the electronic structure of graphene on periodic surfaces [5–11].

One of these 1D periodic structures, the Hex–Au(001) reconstructed structure (shown in Fig. 1), has been studied to apply a 1D periodic potential to graphene and two-dimensional materials [5,12–16]. Au is a prevalent chemical vapor deposition (CVD) substrate for two-dimensional materials such as graphene because of its low chemical activity, high melting point, and low volatility [5,12–21]. Zhou *et al.* reported forming a new Dirac point in graphene grown on Au foil substrate due to the spontaneous formation of Hex–Au(001) 1D periodic potentials [5]. However, the mod-

ulation of the electronic properties was proposed based only on the decrease in the density of states using scanning tunneling spectroscopy, and the band structure of graphene on Hex–Au(001) with respect to the electron momentum is unknown.

Another interesting aspect of graphene on Hex–Au(001) is that while Au has strong spin-orbit interactions, this system lacks spatial inversion symmetry. Therefore, Rashba-type spin polarization can occur at the graphene–Au interface. Spin polarization of graphene is required for the applications in spintronics such as spin-FETs, where the weak spin-orbit interaction of graphene is advantageous [22,23]. This situation is similar to Au-intercalated graphene on Ni(111) and SiC(0001), in which a Rashba splitting of 100 meV was observed due to graphene–Au band hybridization [24,25]. Hex–Au(001) is an excellent example to discuss the hybridization between graphene and Au because previous studies have clarified its structure [26–29], whereas the structure of intercalated Au atoms has not been fully elucidated [24,30]. However, the electronic structure of graphene grown on Hex–Au(001) has not been clarified as previously described.

In the present study, we used angle-resolved photoemission spectroscopy (ARPES) to directly observe the band structure of graphene on a Hex–Au(001) structure. Notably, we used an Au(001) single crystal with a well-defined orientation as the CVD growth substrate to achieve low energy electron diffraction (LEED) and ARPES experiments to determine

*terasawa.tomoo@jaea.go.jp

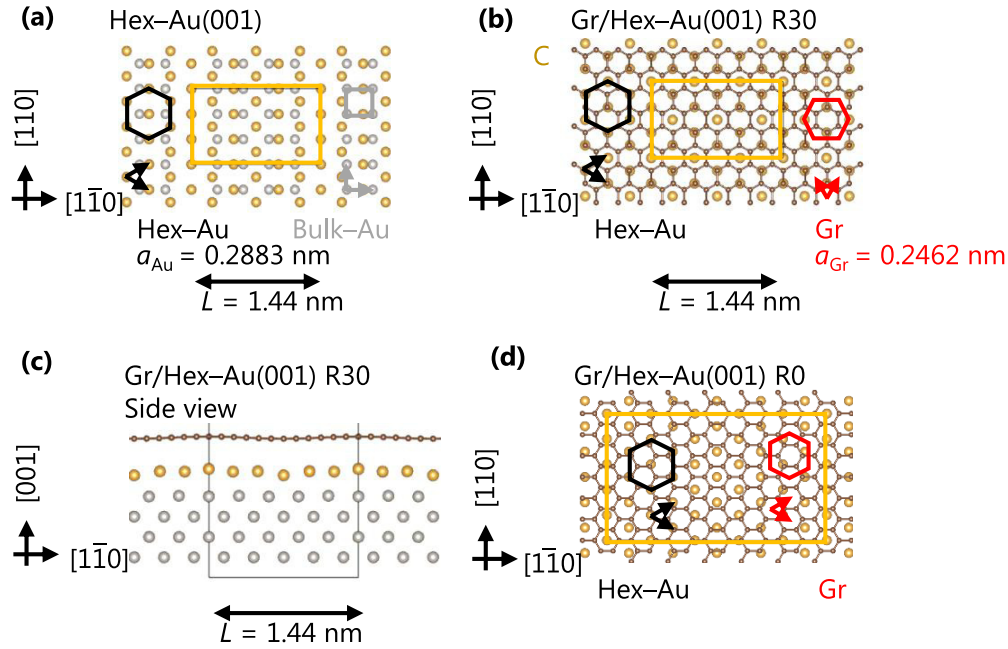


FIG. 1. Schematic illustration of (a) Hex–Au(001) and (b)–(d) graphene (Gr) on the Hex–Au(001) structure. The yellow tetragon with golden balls, the black hexagon with golden balls, and the gray tetragon with gray balls represent the (5×3) superstructure, Hex–Au(001), and bulk Au(001), respectively. The black and gray arrows represent the lattice vectors of Au. In (b), the 90° rotated red hexagon with brown balls depicts the graphene lattice. The red arrows indicate the graphene lattice vector. The graphene lattice is set in the R30 configuration. (c) Sideview of (b). (d) Gr on Hex–Au(001) structure in R0 configuration. $6\sqrt{3} \times 6$ graphene is virtually set on $5\sqrt{3} \times 5$ hexagonal monolayer of Au.

the epitaxial relation of graphene and Au. The electronic structures of graphene and Au were visualized using ARPES measurements at various excitation energies and polarizations. The density functional theory (DFT) calculations based on the experimentally revealed crystal structure showed the electronic band structure consistent with ARPES measurements. Furthermore, we compared the results of the present system with other graphene–Au interfaces and comprehensively discussed the electronic structure of graphene and Au.

II. EXPERIMENTAL PROCEDURE

The apparatus we used for sample preparation is described in detail in Refs. [13,31–33]. Before the graphene growth, the Au(001) single crystal (the substrate for the graphene growth) was cleaned using repeated 2 kV Ar⁺ ion sputtering and vacuum annealing. The Au(001) single crystal was annealed in an Ar atmosphere at 850 °C for 30 min to prepare the Hex–Au(001) surface. The sample temperature was measured using a pyrometer, assuming that the emissivity of the sample was 0.1. Graphene was grown in an Ar atmosphere by adding 3 standard cubic centimeters (sccm) of CH₄ (99.9999% purity) to 250 sccm of Ar (99.9999% purity) at 950 °C. The total pressure was maintained at 10^4 Pa during Hex–Au(001) and graphene formation. The graphene growth time ranged from 15 to 60 min. This study only shows the results of samples with 60 min growth.

Following the fabrication of graphene, the sample was transported through the air to another vacuum chamber and heated at 120 °C for 30 min to eliminate the surface adsorbate for LEED measurements to clarify the orientation relationship between graphene and Au. A 532 nm laser was used as

excitation light for Raman spectroscopy in the air to evaluate the defect density and the number of graphene layers.

ARPES measurements using 21.218 eV (He I α) photon energy were conducted at the Institute for Molecular Science to visualize the graphene and Au band structure. We performed ARPES using different excitation energies and polarization, which affected the selection rule and the matrix element effect [34,35] on the beamlines BL5U and BL7U of the UVSOR-III synchrotron to understand the band structure fully. The results of this study are shown with incident photon energies of $h\nu = 70$ and 30 eV.

In the present study, we performed DFT calculations using the QUANTUM ESPRESSO package [36,37] within the local density approximation (LDA) in order to evaluate the reproducibility of LDA for the preliminary understanding of ARPES results. We used projector-augmented wave pseudopotentials with a Methfessel-Paxton electronic smearing of 0.01 Ry. The kinetic energy cutoff was set at 50 Ry. The k -point sampling was $8 \times 12 \times 1$ Monkhorst–Pack mesh [38]. Figs. 1(a)–1(c) depict the atomic configuration used for DFT calculation, provided by LEED and ARPES results. The structure was visualized using the VESTA package [39]. Figure 1(a) depicts the surface structure of Hex–Au(001), where Au configuration contains the $3\sqrt{3} \times 3$ monolayer of a hexagonal surface lattice and four-layer of a 5×3 bulk square lattice. Since the Au–Au distance is 2.883 Å, the Au 5×3 cell corresponds to approximately 14.42×8.65 Å. The hexagonal lattice on the top surface has a quasi-one-dimensional (Q1D) corrugated structure due to the different lattice parameters of the hexagonal and square lattices in the $[1\bar{1}0]$ direction. In the actual structure, the summits of the corrugation on this

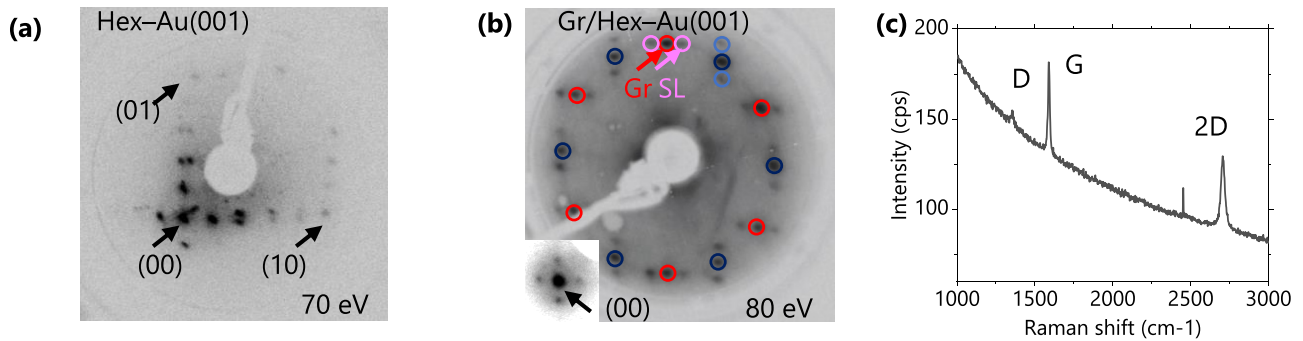


FIG. 2. (a), (b) The LEED pattern of Hex–Au(001) and graphene on the Hex–Au(001) structure. The red and dark blue circles represent the diffraction spots of graphene (Gr), whereas the pink and blue circles represent the superlattice (SL) diffraction spots. The inset in (b) shows the LEED pattern around (00). (c) A typical Raman spectrum of graphene on the Hex–Au(001) structure. The background is also observed due to Au photoluminescence.

surface also exhibit snake-like in-plane corrugation along the [110] direction [26,27]. The surface structure against the bulk was reported to be (5×20) , (5×26) , and so on [26,27]. Hammer *et al.* reported that the actual structure is $c(28 \times 48)$ [28]. However, the periodicity in the $[1\bar{1}0]$ direction can be approximated by $(5 \times n)$, where n is an integer representing the periodicity in the [110] direction [26,29]. For simplicity, we omitted the periodicity of the corrugated structure along the [110] direction in Fig. 1 and considered $(5 \times n)$ periodicity. Figures 1(a)–1(c) assume the simplest case, a (5×3) superstructure.

Graphene covered this surface at a $6 \times 2\sqrt{3}$ orientation [Fig. 1(b)], resulting in a cell size of $14.77 \times 8.53 \text{ \AA}$ as the ring-to-ring distance of graphene is 2.462 \AA . The cell size was fitted to the $6 \times 2\sqrt{3}$ graphene for the DFT calculations because the electronic properties of graphene could be altered when the cell size was fitted to the substrate, as pointed out by Sławińska *et al.* [40]. We optimized the structures based on the stress range below 0.0001 Ry/Bohr . C atoms in graphene, the surface hexagonal Au layer, and the second square Au layer are free, whereas the other square Au layers remain at the bulk positions. After the structural relaxation, the maximum corrugation height of the Au surface along the $[1\bar{1}0]$ direction was 0.64 \AA , which is quantitatively consistent with the 0.65 \AA in the all-electron DFT calculation [26]. This consistency indicated that the Au structure was calculated reliably, even though the cell size fitted to the graphene lattice rather than the Au lattice. The structural relaxation also resulted in the distance between graphene and surface Au being approximately 3.2 \AA , consistent with previous experiments and theoretical calculations for graphene on Au(111) using LDA and DFT-D3 [41,42]. Notably, the DFT calculation using generalized gradient approximation (GGA) showed a longer equilibrium distance of 4.4 \AA in the present calculation, similar to the report by Yortanlı *et al.* [41]. We calculated the band structure after removing the Au square layers and leaving the frozen graphene/Hex–Au configuration to focus the discussion on the interface, as reported by Kang *et al.* [43]. We also calculated the band structures of the isolated hexagonal monolayer of Au and graphene in the same supercell separately to discuss the effect of the hybridization. Due to the limitation of the calculation resource, we set the supercell for the DFT calculation to be $\text{Au } 5 \times 3$, which introduced the periodicity in the

[110] direction to the DFT calculations. This periodicity is unrealistic; therefore, we carefully confirm that we discuss the energy band not originating from the periodicity in the [110] direction.

III. RESULTS

Figure 2(a) shows the LEED pattern of our Hex–Au(001) sample. The diffraction spots exhibit a fivefold periodicity to the bulk square lattice, indicating that the periodicity L corresponds to a quintuple of the interatomic distance in bulk Au. Due to the periodicity along the [110] direction, the second, third, and fourth diffraction spots from the origin were split, whereas the first and fifth were not. The diffraction spots are located every 90° , indicating the double-domain of the Hex–Au(001), because the epitaxial relationship of the surface hexagonal lattice on the bulk square lattice can rotate by 90° . These characteristics are consistent with previous reports [5,27,28]. The domain size was within the electron beam size of LEED, consistent with those in the previous LEED and scanning tunneling microscopy (STM) evaluations being less than 200 nm [5,28]. Furthermore, the LEED results indicate that the Hex–Au(001) structure formed in our sample preparation method remained stable during air transport from the CVD chamber to the LEED chamber.

Graphene was grown on Hex–Au(001) surface by CVD. Figure 2(b) shows the LEED pattern after the CVD growth of graphene. The inset shows the diffraction spots from the superlattice, with a periodicity of $L = 1.44 \text{ nm}$. Figure 2(b) presents graphene-derived diffraction spots (red and dark blue circles) every 30° , and superlattice diffraction spots appear around the graphene diffraction spots (pink and blue circles). The colors were chosen to correspond to 90° rotated double domains. The distance between graphene and superlattice spots was approximately one-sixth of that between graphene spots and the origin, corresponding to the $6 \times 2.462 \text{ \AA} = 14.772 \text{ \AA}$, close to $L = 1.44 \text{ nm}$. This value indicates that superlattice diffractions are generated by the $(5 \times n)$ surface corrugation of Hex–Au(001), which is consistent with previous reports [5,44]. This superlattice diffraction was negligible in an earlier report [5] and unobserved in our sample when grown for a short time. In addition to the sharp spots, a faint ringlike diffraction pattern was observed in Fig. 2(b),

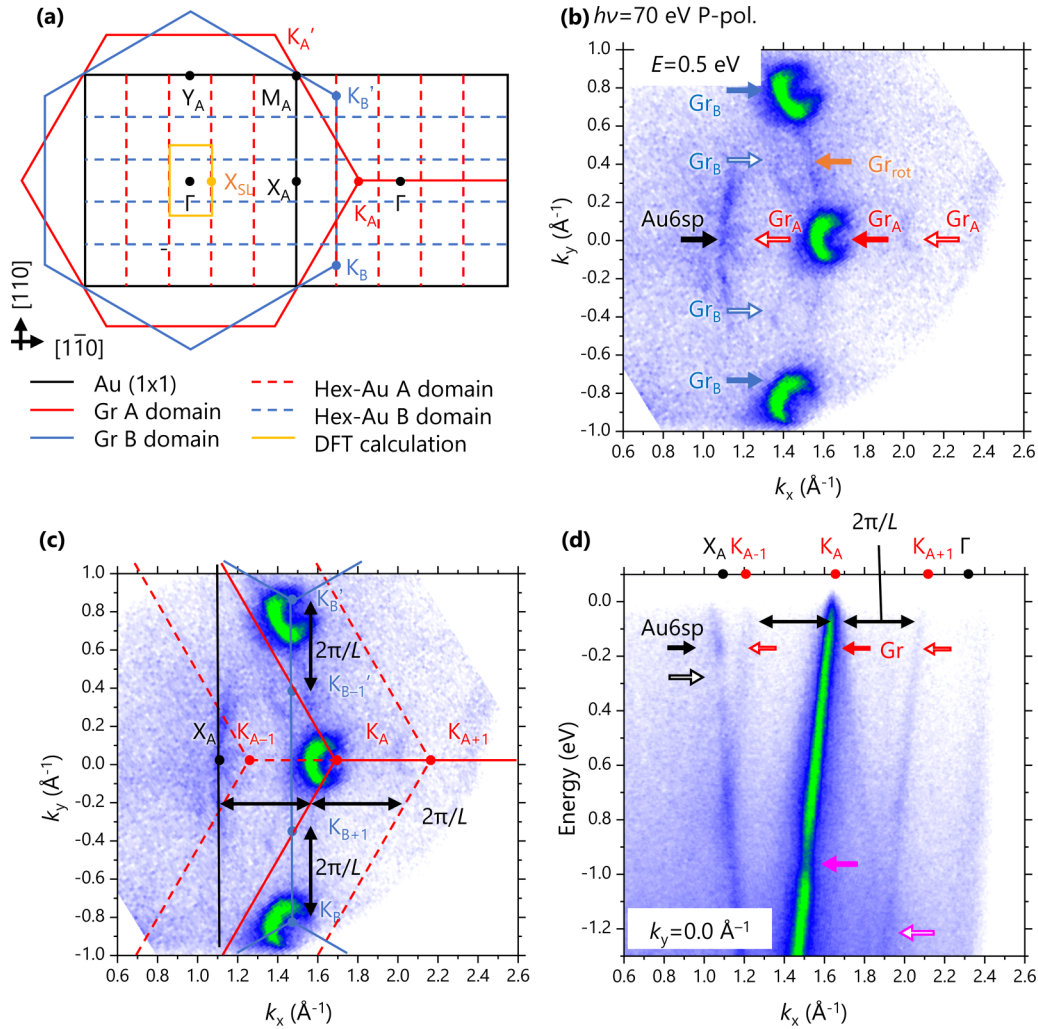


FIG. 3. (a) An illustration of Brillouin zones (BZ). (b), (c) The constant energy contour of the ARPES intensity plot at the binding energy of 0.5 eV around the K_A point. In (c), the BZs are superimposed. The broken red lines indicate the shifted BZ by 0.44 \AA^{-1} , and we named the -0.44 and $+0.44 \text{ \AA}^{-1}$ shifted K_A points as the K_{A-1} and K_{A+1} points, respectively. (d) The ARPES intensity plot is a function of energy along k_x directions. Please see the main text for the definitions of the illustrations and spectral weight.

indicating that a few graphene domains rotated randomly from the epitaxial relation. The short growth time and low-temperature growth increased the ring pattern, indicating that prolonged heating in our sample improved commensuration between graphene and Hex-Au(001).

Below, we discuss the epitaxial relationship between graphene and Au. Graphene growth was reported on the hexagonal Au lattice of the Au(111) surface in R0 and R30 [18]. Figures 1(b) and 1(d) show these epitaxial relations in which the lattice vectors of graphene and Au are parallel and perpendicular, respectively. The twofold symmetry of the superlattice diffractions in Fig. 2(b) indicates that graphene grew in each Hex-Au(001) domain in a single epitaxial relationship. One graphene reciprocal lattice vector is perpendicular to the corrugation periodicity in Fig. 2(b). Conversely, one graphene lattice vector is parallel to the corrugation periodicity $[1\bar{1}0]$ in real space [Fig. 1(b)]. Thus, the lattice vectors of graphene and Au are perpendicular in real space, indicating the R30 relationship between graphene and Hex-Au(001), consistent with previous STM observations of graphene on Hex-Au(001) [5].

Figure 2(c) depicts the typical Raman spectrum of grown graphene. As similar spectra could be obtained everywhere on the sample, the graphene was considered to cover the surface entirely. Three peaks are observed at approximately 1355 , 1590 , and 2707 cm^{-1} , corresponding to D, G, and 2D, respectively [45]. The D and G peaks create A_{1g} and E_{2g} phonons. The D peak is forbidden in a perfect graphene lattice, indicating that this sample contains grain boundaries or defects. The peak intensity ratio of D to G (I_D/I_G) was 0.2. When the excitation laser has a 532-nm wavelength, as in this study, this I_D/I_G value indicates that the domain size of graphene is 100 nm [45]. As discussed in Fig. 1(d), the Hex-Au(001) domain size is 200 nm or less, and the graphene domain size cannot be larger than that [13]. Thus, we concluded that the graphene domain boundary is the primary source of the D band in this sample, and the graphene basal plane is clean, consistent with the clear band dispersion observed in ARPES (Figs. 3–5). The double-resonant Raman scattering process generates the 2D peak [45]. The successful peak fitting of the 2D peak with a single Lorentz function (not shown) indicates that the graphene in this sample is a monolayer [45]. The

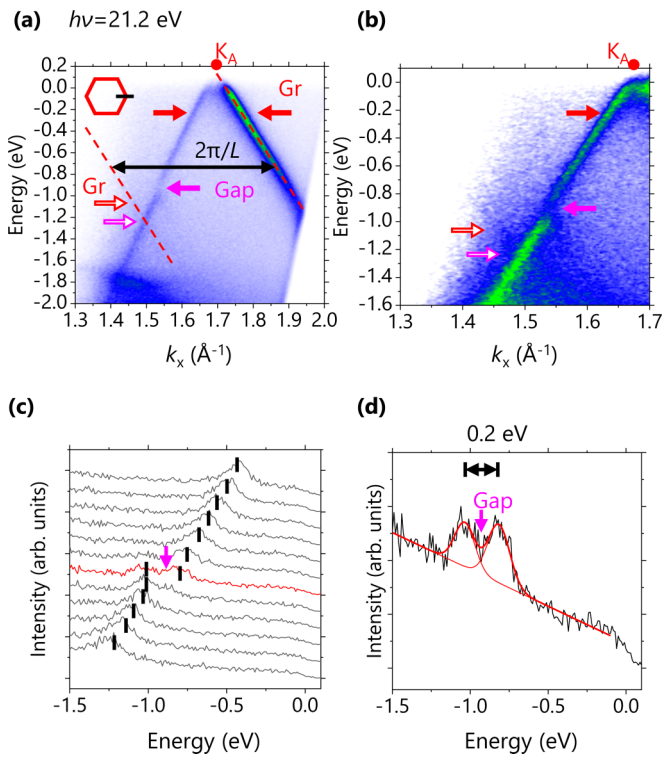


FIG. 4. (a), (b) The ARPES intensity plots along the Γ – K_A line with the He $I\alpha$ light source as a function of k_x and the binding energy. The arrows highlight the feature of the plots in the same way as shown in Fig. 3(d). (c), (d) Energy distribution curves (EDC) of ARPES intensity with a He $I\alpha$ source. Black markers highlight the graphene bands. The purple arrow highlights the energy gap. The red curve shows EDC around the gap ($k_x = 1.545 \text{ \AA}^{-1}$). (d) The EDC was deconvoluted of two Gaussian functions (thin red lines) and a linear background. The thick red line shows the fitting result.

monolayer graphene was grown on the Hex–Au(001) surface in the R30 epitaxy, according to the structural analyses in Fig. 2, and the Hex–Au(001) surface maintained its corrugated structure after graphene growth.

Figure 3 summarizes the entire electronic structure of graphene on Hex–Au(001) observed in ARPES using the 70 eV and P-polarized synchrotron radiation light source. Figure 3(a) depicts the Brillouin zones (BZs) of bulk Au, graphene (A domain), and 90° rotated graphene (B domain) drawn in a black box, red hexagon, and blue hexagon, respectively. The red and blue broken lines represent the periodicity of the Hex–Au(001) reconstruction in the A and B domains. The yellow box shows the BZ corresponding to the unit cell in Fig. 1 used in the DFT calculations. The X point of this BZ is illustrated as the X_{SL} point. The k_x direction was named after the Γ – X_A of Hex–Au(001) periodicity and the Γ – K_A of graphene in the A domain.

Figures 3(b) and 3(c) present the band structure close to the K_A point. In (b), the filled black, filled red (blue), blank red (blue), and filled orange arrows highlight the Au, original graphene in A (B) domains, replica graphene in A (B) domains, and randomly rotated graphene states, respectively. A ringlike state around the K_A point indicates that it is a Dirac cone. Because the incident light was P-polarized, the K–M

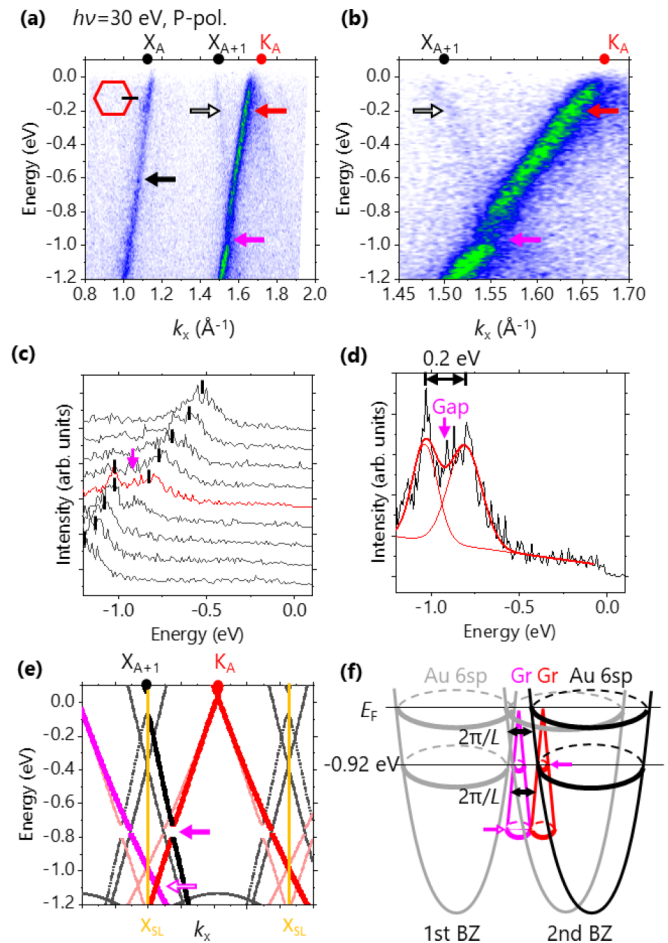


FIG. 5. (a), (b) ARPES intensity plots of graphene on Hex–Au(001) as a function of the binding energy and k_x taken with 30 eV and P-polarized synchrotron radiation light source. The arrows highlight the features of the plot in the same rule as shown in Figs. 3 and 4. (c), (d) EDCs depicted in the same rule as Fig. 4. (e) DFT calculated band structure of graphene on Hex–Au(001). (f) An illustration of the graphene π and Au 6sp bands. The scale of the schematic illustration is arbitrary.

side of the ring was rendered invisible due to the selection rule [34]. Figures 3(b) and 3(c) also present the replica bands of the Dirac cones. The invisible part of the original and replica of the Dirac cones indicates that the original Dirac cone at the K_A point had replicas on the Γ – X_A line, showing the R30 epitaxial relationship between graphene and surface Au, consistent with the LEED results and previous reports [5,18]. The distance between the original and replica bands is approximately $2\pi/L = 0.44 \text{ \AA}^{-1}$, corresponding to a periodicity L of 1.44 nm.

The spectral weight is observed at 1.1 \AA^{-1} from the Γ point in the first BZ of Au at $E = 0.5 \text{ eV}$. We assigned them to the Au 6sp band because it was similar to that observed in the bare Hex–Au(001), indicating that the electronic structure of Hex–Au(001) was preserved after the graphene growth [12]. The Au 6sp band is a paraboloid of revolution centering the Γ point; thus, its curvature suggests that this band originated from the Γ points of the second BZ. This characteristic is also reported on Hex–Au(001) [27].

The linear dispersion, which is the characteristic of the Dirac cone, is also observed around the K_A point in the ARPES intensity plot using the P-polarized light source shown in Fig. 3(d), whereas Fig. S1 in the Supplemental Material shows the data obtained using the S-polarized light source [46]. The filled black, filled red, and blank red arrows highlight the original Au $6sp$, original graphene, and replica graphene bands, respectively. The periodicity of $2\pi/L$ is highlighted in the k_x direction. Although the P-polarization was used for the incident light, a faint state in the K–M direction was observed in addition to the robust one in the Γ –K direction [34]. The Dirac point is estimated from the extrapolation of the linear dispersions in the Γ –K and K–M directions to be 0.18 eV higher than the Fermi energy, indicating that graphene donates electrons to Au. This value is close to the electron donation degree from graphene to Au(111) [18,47], despite the corrugation of the Hex–Au(001) topmost surface. The blank black arrow highlights the gap in the Au $6sp$ band. In the Supplemental Material [46], the detail of the Au $6sp$ band structure is discussed using the ARPES intensity plot in the k_y direction (Fig. S2). Notably, this Au $6sp$ band can be assigned to the Y_B point. We will discuss whether or not the Au $6sp$ band in the A domain was observed in Fig. 5.

The most exciting feature in the graphene band is the anomaly at $(k_x, E) = (1.55 \text{ \AA}^{-1}, -0.9 \text{ eV})$ [the filled purple arrow in Fig. 3(d)]. We discussed its origin in Figs. 4 and 5. Figures 4(a) and 4(b) depict the ARPES image with the He $I\alpha$ light source. The Γ –K and K–M sides of the Dirac cone were visible because the incident light was unpolarized. The graphene bands show a gaplike feature, highlighted by a purple arrow in Figs. 4(a) and 4(b). The energy distribution curve (EDC) in Figs. 4(c) and 4(d) showed two peaks around the gap ($k_x = 1.545 \text{ \AA}^{-1}$), where the peak positions were -0.82 and -1.04 eV. We thus concluded that graphene on Hex–Au(001) showed an energy gap of 0.2 eV centering at -0.93 eV.

Previously, a 1D-periodic potential was considered the origin of the bandgap formation in graphene π bands on Hex–Au(001) [1,5]. Thus, the crossing point of the original and replica graphene bands should show an anomaly [1]. Figure 4(b) shows a faint band highlighted by a blank red arrow crossing the π band of graphene at $(k_x, E) = (1.50 \text{ \AA}^{-1}, -1.2 \text{ eV})$. The relative momentum difference of this band is 0.4 \AA^{-1} from the graphene π band of the K–M direction ($k_x, E) = (1.90 \text{ \AA}^{-1}, -1.2 \text{ eV})$ shown in Fig. 4(a). We attributed this band to the replica band of graphene. However, the crossing point of the replica and original bands shows no gap [the blank purple arrows in Figs. 3(d), 4(a), and 4(b)], although the symmetries of those graphene bands should be the same. One possibility is that the 1D periodic potential of the Hex–Au(001) could be too small to create the observable bandgap because the periodic potential height determines the bandgap size [1]. Another explanation is that the replica graphene π band appeared due to the final state effect [48]. In this case, the replica band appears due to the diffraction of the photoelectron, and the periodic potential does not modulate the graphene band structure. The modification of the electronic structure of graphene by the 1D periodic potential of the Hex–Au(001) requires further research.

In order to discuss the origin of the gap in the graphene π band, we analyzed the gap structure using 30 eV and P-polarized synchrotron radiation light source in Figs. 5(a)–5(d). Significant bands around the X_A and K_A points appear in Fig. 5(a), corresponding to the Au $6sp$ and graphene π bands discussed in this paper. A faint dispersive band was also observed around the X_{A+1} point, which is the $+0.44 \text{ \AA}^{-1}$ shifted X_A point. We attribute this band to a replica of the Au $6sp$ band. The replica Au $6sp$ meets the original graphene π bands at $(k_x, E) = (1.56 \text{ \AA}^{-1}, -0.78 \text{ eV})$ in Fig. 5(b). We also analyzed Fig. 5(a) by making the EDCs in Figs. 5(c) and 5(d). The peak positions were -0.81 and -1.04 eV. As a result, the upper band positions in Figs. 4 and 5 are quantitatively consistent. Thus, we concluded that the bandgap formed at the crossing point of graphene π and replica Au $6sp$, and the origin of the graphene π bandgap is the hybridization between graphene π and Au $6sp$ bands. The hybridization between the original graphene π and replica Au $6sp$ bands indicates that the replica Au $6sp$ band appears not due to the final state effect. From the viewpoint of symmetry, the mirror inversion on the zx plane should be considered in the symmetry operation for the bands on the k_x line. Both graphene π and Au $6sp$ bands are symmetric to the mirror inversion for the zx plane; therefore, hybridization between these bands is plausible. The gap structure along the k_y direction is also analyzed in Fig. S3 of the Supplemental Material [46]. Notably, the replica Au $6sp$ band around the X_{A+1} point must be in the A domain, in contrast to the original Au $6sp$ band in Fig. 3, which is assigned to the B domain. This is one of the reasons that we discuss the crossing point of the original graphene π and replica Au $6sp$ bands. The slope of the Au $6sp$ band around the X_{A+1} point in Fig. 5(a) was 11.0 eV \AA^{-1} , while that of the Au $6sp$ bands in Figs. 3(d) and S1, belonging to the B domain, were approximately 9.3 eV \AA^{-1} . As the slope of the Au $6sp$ band around k_x of 1.1 \AA^{-1} in Fig. 5(a) was 8.5 eV \AA^{-1} , we assigned this band to the B domain. We attribute the different slopes to the asymmetry of the Au $6sp$ bands between the Γ – X_A and Γ – Y_B directions and/or the effect of the hybridization with the graphene π band. In the present study, we observed original Au $6sp$ bands only in the B domain in Figs. 3(d), S1, and 5(a). The observation of the Au $6sp$ band in the A domain was achieved only for its replica by changing the polarization and energy of the incident light. We attributed these results to the matrix element effect that affects the ARPES intensity of the bands depending on the incident light.

Figure 5(e) depicts the theoretically calculated band structure along k_x to discuss the bandgap formation of the graphene π band. The red, pink, and purple plots show graphene, while the gray and black plots represent Au. We used red and purple plots for the original and replica Dirac cone due to the periodicity along the k_x direction. Black plots were used to highlight the Au $6sp$ band around the gap. Yellow lines show the BZ of the supercell. Notably, the crossing point of the original graphene π and Au $6sp$ bands was heavily overlapped by Au $5d$, as shown in Fig. S4 in the Supplemental Material [46]. Thus, we discussed the relatively shallow energy region. In Fig. 5(e), the π bands of graphene (red and purple plots) cross without any energy gap, consistent with Fig. 4. The absence of a gap in the DFT calculations indicates that even if the replica graphene π band in Fig. 4(b) originates from the initial state

effect, the energy potential generated by the Au corrugation is considered insufficient to modulate the electronic structure of graphene. Moreover, a 0.1 eV energy gap was formed around the crossing point between graphene π and Au $6sp$ bands (red and black plots) at -0.8 eV, qualitatively consistent with the observed bands in ARPES shown in Figs. 3(d), 4(a), 4(b), 5(a), and 5(b). Therefore, DFT calculations indicate that the origin of bandgap formation was not the periodic potential of the surface corrugation but rather the hybridization between graphene π and Au $6sp$ bands. However, the bandgap positions in the energy axis obtained from experiments and calculations are quantitatively inconsistent. Further calculations, especially ones accounting for van der Waals interaction (for example, GGA + vdW could improve the results quantitatively) and the relativistic effect, are required to illustrate the band structure of graphene on Hex–Au(001) structures.

Figure 5(f) summarizes the relation between original and replica graphene and Au bands. The Dirac cone of graphene was represented by a red cone. This band has a replica Dirac cone represented by the purple cone. A blank purple arrow highlights the intersection of the red and purple cones, where the gap was not observed. The gray parabolas represent the original Au $6sp$ bands centering at the Γ points in the first and second BZs, accompanied by the replica Au $6sp$ band represented by the black parabola. This replica band crosses the original Dirac cone, highlighted by a filled purple arrow, where the gap was observed.

IV. DISCUSSION

This study found the hybridization between graphene and Au on Hex–Au(001). We discuss the consistency and inconsistency of our results with the previous experimental and theoretical reports [24,25,40,49]. A large Rashba splitting of 100 meV in the graphene π band was reported for Au-intercalated graphene on the Ni(111) system due to the hybridization with Au $5d$ bands around binding energy of 5 eV [24,30,50–55]. However, Au $6sp$ does not hybridize with the graphene π band in this system. Other systems, such as Au-intercalated graphene on Ru(0001) and Re(0001), do not exhibit hybridization between graphene and Au $6sp$ [56–58]. Au atoms grew epitaxially to the substrates in those systems, resulting in the hexagonal lattice. The epitaxial relations between graphene and intercalated Au were R0 [imaginary shown in Fig. 1(d)], whereas the structure of intercalated Au is under discussion [24,30]. Although a large supercell (8×8 or 9×9) was necessary to accommodate the large (approximately 10%) lattice mismatch of graphene and Au in R0 relation, theoretical calculations have shown that these systems would not result in graphene and Au $6sp$ hybridization for Au intercalation [59–61]. We speculate that such a significant lattice mismatch might result in insufficient graphene and Au orbitals overlap.

To the best of our knowledge, graphene and Au $6sp$ hybridization was reported for the first time in the Au-intercalated graphene on SiC(0001) system [25]. The R30 epitaxial relation describes the similarity of graphene on Hex–Au(001) to Au-intercalated graphene on SiC(0001) systems [62]. Thus, we discussed the consistency of these references to our results. In Au-intercalated graphene on

SiC(0001), the doping level of graphene is $+0.1$ eV, similar to our results [25,62]. They also observed gap openings at -1.1 and -1.9 eV. The authors attributed these to the hybridization with the Au $6sp$ band [25] based on DFT calculation [24]. We agree with the conclusion but disagree with its process because the calculated band structure of the graphene and Au interface was in the R0 relation [24]. Unfortunately, their ARPES measurement uses the angle resolution of 1° , which is insufficient for discussing the faint bands due to the development of Au $6sp$, which can hybridize with graphene π bands. Presumably, due to this limitation, the electronic structure of Au $6sp$ was not clarified in Ref. [25].

Forti *et al.* used ARPES to investigate the electronic structure of Au-intercalated graphene on SiC(0001) [62]. The p-type Au-intercalated graphene reported the energy gap at -1.1 eV in the k_y direction (perpendicular to the Γ –K line). They attribute its origin to the interaction with the Au $6sp$ band [62], according to Ref. [25]. We also observed the gap at -0.9 eV in the k_y direction, as shown in Fig. S5 in the Supplemental Material [46]. Thus, our findings are qualitatively consistent with their reports. However, quantitatively, the gap position along the energy direction is not the same, presumably due to the difference between the electronic structures of Au $6sp$ in Hex–Au(001) and Au intercalated graphene on SiC: the former has 1D corrugated in 0.6 \AA , while the latter has a 2D moiré structure in 2 \AA height. These results mean that the hybridization gap with Au $6sp$ locates around -1 eV, and its position is affected by the periodicity of the Au hexagonal lattice. We expect the shallow and tunable gap position to be promising for spin injection into graphene for spin-FET. Further experiments using spin-resolved ARPES are required to reveal the spin characteristics of graphene and Au interfaces, including Au-intercalated graphene on SiC(0001) and graphene on Hex–Au(001).

Many DFT calculations were conducted for the R30 configuration of graphene and Au hexagonal lattices, as this structure requires only a 2×2 supercell [40,41,43,49,63]. The calculated band structures for R30 are not always consistent with the experimental and theoretical results for R0, as pointed out by Voloshina and Dedkov [60]. However, discussing the band structure of graphene on Hex–Au(001) is reliable as its epitaxial relation is understood to be R30 [5]. The calculated band structures for the R30 configuration showed that the energy gap in the graphene π band formed due to graphene π and Au $6sp$ band hybridization [40,41,43,49,63]. These experimental and theoretical results indicate that the R30 configuration is essential for hybridization and band-gap formation. The R30 configuration resulted in the on-top relation for some C and Au atoms, as shown in Fig. 1(b). Therefore, Au and C atoms were spatially close to each other in the R30 configuration for graphene on the Hex–Au(001) surface, resulting in overlapping orbitals hybridizing to create the band gap in the graphene π band.

In addition to graphene on Hex–Au(001) and Au-intercalated graphene on SiC(0001), graphene on the Au(111) surface experimentally showed R30 (and R0) epitaxial relations and no visible bandgap in the π band [18]. Although R0 epitaxial graphene on Au(111) does not exhibit hybridization for the reasons stated above, R30 graphene on Au(111) could result in graphene and Au $6sp$ hybridization and

bandgap formation. Previous DFT calculations for graphene on Au(111) showed hybridization and bandgap formation between graphene and Au $6sp$, contradicting previous experimental results [18,40,41,43,49]. The critical difference in the electronic structures between Au(111) and Hex–Au(001) is that in the Hex–Au(001), the symmetries of the surface and bulk are different, isolating the electronic structure in the Au hexagonal lattice from the bulk [5,27]. Thus, we suspect that the isolated electronic structure of the hexagonal Au lattice interacts strongly with graphene. Further theoretical studies are required to understand the interaction between graphene and the Au(111) surface in the R30 configuration. We anticipate that our results for graphene on Hex–Au(001) will be helpful for further research as its epitaxial relation is fixed to R30.

V. CONCLUSIONS

We prepared graphene on a Hex–Au(001) surface using CVD while maintaining its corrugated structure. LEED and ARPES revealed that the epitaxial relationship between graphene and Au is R30. The band structure of graphene on the Hex–Au(001) surface was observed using ARPES, discussed using DFT calculation, and no gap was found at the crossing point of graphene π bands. The 1D potential created by the Au corrugation of 0.6 \AA appeared to be too small to

create the bandgap. Conversely, we observed the hybridization between graphene and Au $6sp$ and a large bandgap of 0.2 eV (0.1 eV) in ARPES (DFT). We discussed the graphene and hexagonal Au interfaces in R0 and R30 epitaxial relations compared with previous reports and concluded that the R30 relation is critical for hybridizing graphene π and Au $6sp$ bands. The Au electronic structure isolated from the bulk also seems necessary to interact with graphene. We anticipate that a similar electronic structure of graphene on Hex–Au(001) to that of other graphene and Au interfaces will result in the spin characteristics even in graphene on Hex–Au(001).

ACKNOWLEDGMENTS

The authors are grateful for the experimental assistance by beamline staff at BL5U and BL7U of UVSOR-III synchrotron radiation facility. Dr. S. Machida and Dr. M. Yano helped with the LEED measurements. The authors acknowledge Dr. T. U. Ito for supporting the theoretical calculations. The present work was supported by JSPS KAKENHI (Grant No. 19K15400). T. T. acknowledges the funding from Konica Minolta Science and Technology Foundation. T. I. acknowledges support from JSPS KAKENHI (Grant No. 17K05495). The ARPES experiments using synchrotron light were conducted at UVSOR-III BL5U (Proposals No. 19-848, No. 20-763) and BL7U (Proposals No. 19-862, No. 20-862, and No. 20-783).

-
- [1] C.-H. Park, L. Yang, Y.-W. Son, M. L. Cohen, and S. G. Louie, Anisotropic behaviours of massless Dirac fermions in graphene under periodic potentials, *Nat. Phys.* **4**, 213 (2008).
 - [2] B. Hunt, J. D. Sanchez-Yamagishi, A. F. Young, M. Yankowitz, B. J. LeRoy, K. Watanabe, T. Taniguchi, P. Moon, M. Koshino, P. Jarillo-Herrero *et al.*, Massive Dirac fermions and Hofstadter butterfly in a van der Waals heterostructure, *Science* **340**, 1427 (2013).
 - [3] Y. Cao, V. Fatemi, S. Fang, K. Watanabe, T. Taniguchi, E. Kaxiras, and P. Jarillo-Herrero, Unconventional superconductivity in magic-angle graphene superlattices, *Nature (London)* **556**, 43 (2018).
 - [4] W. Yang, G. Chen, Z. Shi, C.-C. Liu, L. Zhang, G. Xie, M. Cheng, D. Wang, R. Yang, D. Shi *et al.*, Epitaxial growth of single-domain graphene on hexagonal boron nitride, *Nat. Mater.* **12**, 792 (2013).
 - [5] X. Zhou, Y. Qi, J. Shi, J. Niu, M. Liu, G. Zhang, Q. Li, Z. Zhang, M. Hong, Q. Ji *et al.*, Modulating the electronic properties of monolayer graphene using a periodic quasi-one-dimensional potential generated by hex-reconstructed Au(001), *ACS Nano* **10**, 7550 (2016).
 - [6] A. Locatelli, C. Wang, C. Africh, N. Stojić, T. O. Menteş, G. Comelli, and N. Binggeli, Temperature-Driven reversible rippling and bonding of a graphene superlattice, *ACS Nano* **7**, 6955 (2013).
 - [7] M. Pizarra, D. Pacilé, P. Moras, P. M. Sheverdyaeva, A. Sindona, M. Papagno, and C. Carbone, Electronic structure of epitaxial graphene grown on stepped Pt(997), *Phys. Rev. B* **89**, 195438 (2014).
 - [8] W.-J. Jang, M. W. Lee, H. Kim, S. Park, S. J. Jung, S. Lee, Y. J. Song, and S.-J. Kahng, Observations of new Dirac points in one-dimensionally-rippled graphene on hexagonal BN using scanning tunneling spectroscopy, *J. Phys. Chem. C* **119**, 19535 (2015).
 - [9] M. Kralj, F. Craes, W. Sun, M.-C. Asensio, P. Lazic, I. Šrut Rakić, J. Avila, W. Jolie, C. Busse, V. Mikšić Trontl *et al.*, Step-induced faceting and related electronic effects for graphene on Ir(332), *Carbon* **110**, 267 (2016).
 - [10] A. Celis, M. N. Nair, M. Sicot, F. Nicolas, S. Kubsky, D. Malterre, A. Taleb-Ibrahimi, and A. Tejada, Superlattice-Induced minigaps in graphene band structure due to underlying one-dimensional nanostructuring, *Phys. Rev. B* **97**, 195410 (2018).
 - [11] A. Sala, Z. Zou, V. Carnevali, M. Panighel, F. Genuzio, T. O. Menteş, A. Locatelli, C. Cepek, M. Peressi, G. Comelli *et al.*, Quantum confinement in aligned zigzag “Pseudo-Ribbons” embedded in graphene on Ni(100), *Adv. Funct. Mater.* **32**, 2105844 (2022).
 - [12] J. Shi, X. Zhang, D. Ma, J. Zhu, Y. Zhang, Z. Guo, Y. Yao, Q. Ji, X. Song, Y. Zhang *et al.*, Substrate facet effect on the growth of monolayer MoS₂ on Au foils, *ACS Nano* **9**, 4017 (2015).
 - [13] T. Terasawa, T. Taira, S. Yasuda, S. Obata, K. Saiki, and H. Asaoka, Effect of hydrogen on chemical vapor deposition growth of graphene on Au substrates, *Jpn. J. Appl. Phys.* **58**, SIIB17 (2019).
 - [14] M. Hong, X. Zhou, J. Shi, Y. Qi, Z. Zhang, Q. Fang, Y. Guo, Y. Sun, Z. Liu, Y. Li *et al.*, Quasi-Freestanding, striped WS₂

- monolayer with an invariable band gap on Au(001), *Nano Res.* **10**, 3875 (2017).
- [15] X. Zhou, J. Shi, Y. Qi, M. Liu, D. Ma, Y. Zhang, Q. Ji, Z. Zhang, C. Li, Z. Liu *et al.*, Periodic modulation of the doping level in striped MoS₂ superstructures, *ACS Nano* **10**, 3461 (2016).
- [16] Q. Wu, X. Fu, K. Yang, H. Wu, L. Liu, L. Zhang, Y. Tian, L. J. Yin, W. Q. Huang, W. Zhang *et al.*, Promoting a weak coupling of monolayer MoSe₂ grown on (100)-Faceted Au foil, *ACS Nano* **15**, 4481 (2021).
- [17] T. Oznuher, E. Pince, E. O. Polat, O. Balci, O. Salihoglu, and C. Kocabas, Synthesis of graphene on gold, *Appl. Phys. Lett.* **98**, 183101 (2011).
- [18] J. M. Wofford, E. Starodub, A. L. Walter, S. Nie, A. Bostwick, N. C. Bartelt, K. Thürmer, E. Rotenberg, K. F. McCarty, and O. D. Dubon, Extraordinary epitaxial alignment of graphene islands on Au(111), *New J. Phys.* **14**, 053008 (2012).
- [19] S. Nie, N. C. Bartelt, J. M. Wofford, O. D. Dubon, K. F. McCarty, and K. Thürmer, Scanning tunneling microscopy study of graphene on Au(111): Growth mechanisms and substrate interactions, *Phys. Rev. B* **85**, 205406 (2012).
- [20] S. Yasuda, R. Kumagai, K. Nakashima, and K. Murakoshi, Electrochemical potential stabilization of reconstructed Au(111) structure by monolayer coverage with graphene, *J. Phys. Chem. Lett.* **6**, 3403 (2015).
- [21] S. Yasuda, R. Takahashi, R. Osaka, R. Kumagai, Y. Miyata, S. Okada, Y. Hayamizu, and K. Murakoshi, Out-of-plane strain induced in a moiré superstructure of monolayer MoS₂ and MoSe₂ on Au(111), *Small* **13**, 1700748 (2017).
- [22] Y. G. Semenov, K. W. Kim, and J. M. Zavada, Spin field effect transistor with a graphene channel, *Appl. Phys. Lett.* **91**, 153105 (2007).
- [23] N. Tombros, C. Jozsa, M. Popinciuc, H. T. Jonkman, and B. J. van Wees, Electronic spin transport and spin precession in single graphene layers at room temperature, *Nature (London)* **448**, 571 (2007).
- [24] D. Marchenko, A. Varykhalov, M. R. Scholz, G. Bihlmayer, E. I. Rashba, A. Rybkin, A. M. Shikin, and O. Rader, Giant Rashba splitting in graphene due to hybridization with gold, *Nat. Commun.* **3**, 1232 (2012).
- [25] D. Marchenko, A. Varykhalov, J. Sánchez-Barriga, T. Seyller, and O. Rader, Rashba splitting of 100 meV in Au-intercalated graphene on SiC, *Appl. Phys. Lett.* **108**, 172405 (2016).
- [26] P. Havu, V. Blum, V. Havu, P. Rinke, and M. Scheffler, Large-Scale surface reconstruction energetics of Pt(100) and Au(100) by all-electron density functional theory, *Phys. Rev. B* **82**, 161418(R) (2010).
- [27] S. Bengió, V. Navarro, M. A. González-Barrio, R. Cortés, I. Vobornik, E. G. Michel, and A. Mascaraque, Electronic structure of reconstructed Au(100): Two-dimensional and one-dimensional surface states, *Phys. Rev. B* **86**, 045426 (2012).
- [28] R. Hammer, A. Sander, S. Förster, M. Kiel, K. Meinel, and W. Widdra, Surface reconstruction of Au(001): High-resolution real-space and reciprocal-space inspection, *Phys. Rev. B* **90**, 035446 (2014).
- [29] A. Trembulowicz, B. Pieczyrak, L. Jurczyszyn, and G. Antczak, Coexistence of Nanowire-like hex and (1 × 1) phases in the topmost layer of Au(100) surface, *Nanotechnology* **30**, 045704 (2019).
- [30] M. Krivenkov, E. Golias, D. Marchenko, J. Sánchez-Barriga, G. Bihlmayer, O. Rader, and A. Varykhalov, Nanostructural origin of giant Rashba effect in intercalated graphene, *2D Mater.* **4**, 035010 (2017).
- [31] T. Terasawa and K. Saiki, Radiation-Mode optical microscopy on the growth of graphene, *Nat. Commun.* **6**, 6834 (2015).
- [32] T. Terasawa and K. Saiki, Effect of vapor-phase oxygen on chemical vapor deposition growth of graphene, *Appl. Phys. Express* **8**, 035101 (2015).
- [33] T. Taira, S. Obata, and K. Saiki, Nucleation site in CVD graphene growth investigated by radiation-mode optical microscopy, *Appl. Phys. Express* **10**, 055502 (2017).
- [34] E. L. Shirley, L. J. Terminello, A. Santoni, and F. J. Himpsel, Brillouin-zone-selection effects in graphite photoelectron angular distributions, *Phys. Rev. B* **51**, 13614 (1995).
- [35] J. J. Yeh and I. Lindau, Atomic subshell photoionization cross sections and asymmetry Parameters: $1 \leq z \leq 103$, *At. Data Nucl. Data Tables* **32**, 1 (1985).
- [36] P. Giannozzi, S. Baroni, N. Bonini, M. Calandra, R. Car, C. Cavazzoni, D. Ceresoli, G. L. Chiarotti, M. Cococcioni, I. Dabo *et al.*, QUANTUM ESPRESSO: A modular and open-source software project for quantum simulations of materials, *J. Phys. Condens. Matter* **21**, 395502 (2009).
- [37] P. Giannozzi, O. Andreussi, T. Brumme, O. Bunau, M. Buongiorno Nardelli, M. Calandra, R. Car, C. Cavazzoni, D. Ceresoli, M. Cococcioni *et al.*, Advanced capabilities for materials modelling with QUANTUM ESPRESSO, *J. Phys.: Condens. Matter* **29**, 465901 (2017).
- [38] H. J. Monkhorst and J. D. Pack, Special points for Brillouin-zone integrations, *Phys. Rev. B* **13**, 5188 (1976).
- [39] K. Momma and F. Izumi, VESTA 3 for three-dimensional visualization of crystal, volumetric, and morphology data, *J. Appl. Crystallogr.* **44**, 1272 (2011).
- [40] J. Sławińska, P. Dabrowski, and I. Zasada, Doping of graphene by a Au(111) Substrate: Calculation strategy within the local density approximation and a semiempirical van der Waals approach, *Phys. Rev. B* **83**, 245429 (2011).
- [41] M. Yortanlı and E. Mete, Common surface structures of graphene and Au(111): The effect of rotational angle on adsorption and electronic properties, *J. Chem. Phys.* **151**, 214701 (2019).
- [42] S. Yasuda, K. Tamura, T. Terasawa, M. Yano, H. Nakajima, T. Morimoto, T. Okazaki, R. Agari, Y. Takahashi, M. Kato *et al.*, Confinement of hydrogen molecules at graphene–metal interface by electrochemical hydrogen evolution reaction, *J. Phys. Chem. C* **124**, 5300 (2020).
- [43] M. H. Kang, S. C. Jung, and J. W. Park, Density functional study of the Au-intercalated Graphene/Ni(111) surface, *Phys. Rev. B* **82**, 085409 (2010).
- [44] L. Nilsson, M. Andersen, J. Bjerre, R. Balog, B. Hammer, L. Hornekær, and I. Stensgaard, Preservation of the Pt(100) surface reconstruction after growth of a continuous layer of graphene, *Surf. Sci.* **606**, 464 (2012).
- [45] A. C. Ferrari, Raman spectroscopy of graphene and Graphite: Disorder, electron-phonon Coupling, doping and nonadiabatic effects, *Solid State Commun.* **143**, 47 (2007).
- [46] See Supplemental Material at <http://link.aps.org/supplemental/10.1103/PhysRevMaterials.7.014002> for the S-polarized version of Fig. 3(d), details of the Au 6s*p* band structure, k_y cuts of the hybridization gap, DFT calculated band structure without hybridization, and k_y cut of the Dirac cone.

- [47] G. Giovannetti, P. A. Khomyakov, G. Brocks, V. M. Karpan, J. van den Brink, and P. J. Kelly, Doping Graphene with Metal Contacts, *Phys. Rev. Lett.* **101**, 026803 (2008).
- [48] C. M. Polley, L. I. Johansson, H. Fedderwitz, T. Balasubramanian, M. Leandersson, J. Adell, R. Yakimova, and C. Jacobi, Origin of the π -Band replicas in the electronic structure of graphene grown on 4H-SiC(0001), *Phys. Rev. B* **99**, 115404 (2019).
- [49] P. A. Khomyakov, G. Giovannetti, P. C. Rusu, G. Brocks, J. van den Brink, and P. J. Kelly, First-Principles study of the interaction and charge transfer between graphene and metals, *Phys. Rev. B* **79**, 195425 (2009).
- [50] A. M. Shikin, G. V. Prudnikova, V. K. Adamchuk, F. Moresco, and K. H. Rieder, Surface intercalation of gold underneath a graphite monolayer on Ni(111) studied by angle-resolved photoemission and high-resolution electron-energy-loss spectroscopy, *Phys. Rev. B* **62**, 13202 (2000).
- [51] A. Varykhalov, J. Sánchez-Barriga, A. M. Shikin, C. Biswas, E. Vescovo, A. Rybkin, D. Marchenko, and O. Rader, Electronic and Magnetic Properties of Quasifreestanding Graphene on Ni, *Phys. Rev. Lett.* **101**, 157601 (2008).
- [52] A. Varykhalov, M. R. Scholz, T. K. Kim, and O. Rader, Effect of noble-metal contacts on doping and band gap of graphene, *Phys. Rev. B* **82**, 121101(R) (2010).
- [53] A. M. Shikin, A. G. Rybkin, D. Marchenko, A. A. Rybkina, M. R. Scholz, O. Rader, and A. Varykhalov, Induced spin-orbit splitting in Graphene: The role of atomic number of the intercalated metal and π -d hybridization, *New J. Phys.* **15**, 013016 (2013).
- [54] E. V. Zhizhin, A. Varykhalov, A. G. Rybkin, A. A. Rybkina, D. A. Pudikov, D. Marchenko, J. Sánchez-Barriga, I. I. Klimovskikh, G. G. Vladimirov, O. Rader *et al.*, Spin splitting of Dirac fermions in graphene on Ni intercalated with alloy of Bi and Au, *Carbon* **93**, 984 (2015).
- [55] I. Gierz, T. Suzuki, R. T. Weitz, D. S. Lee, B. Krauss, C. Riedl, U. Starke, H. Höchst, J. H. Smet, C. R. Ast *et al.*, Electronic decoupling of an epitaxial graphene monolayer by gold intercalation, *Phys. Rev. B* **81**, 235408 (2010).
- [56] S. Günther, T. O. Menteş, R. Reichelt, E. Miniussi, B. Santos, A. Baraldi, and A. Locatelli, Au intercalation under epitaxial graphene on Ru(0001): The role of graphene edges, *Carbon* **162**, 292 (2020).
- [57] E. Mazaleyrat, S. Vlaic, A. Artaud, L. Magaud, T. Vincent, A. C. Gómez-Herrero, S. Lisi, P. Singh, N. Bendiab, V. Guisset *et al.*, How to induce superconductivity in epitaxial graphene via remote proximity effect through an intercalated gold layer, *2D Mater.* **8**, 015002 (2020).
- [58] C. Enderlein, Y. S. Kim, A. Bostwick, E. Rotenberg, and K. Horn, The formation of an energy gap in graphene on ruthenium by controlling the interface, *New J. Phys.* **12**, 033014 (2010).
- [59] J. Sławińska and J. I. Cerdá, Complex spin texture of Dirac cones induced via spin-orbit proximity effect in graphene on metals, *Phys. Rev. B* **98**, 075436 (2018).
- [60] E. Voloshina and Y. Dedkov, Realistic large-scale modeling of rashba and induced spin-orbit effects in graphene/high-z-metal systems, *Adv. Theory Simul.* **1**, 1800063 (2018).
- [61] J. Sławińska and J. I. Cerdá, Spin-orbit proximity effect in graphene on metallic substrates: Decoration versus intercalation with metal adatoms, *New J. Phys.* **21**, 073018 (2019).
- [62] S. Forti, S. Link, A. Stöhr, Y. Niu, A. A. Zakharov, C. Coletti, and U. Starke, Semiconductor to metal transition in two-dimensional gold and its van der Waals heterostack with graphene, *Nat. Commun.* **11**, 2236 (2020).
- [63] F.-C. Chuang, W.-H. Lin, Z.-Q. Huang, C.-H. Hsu, C.-C. Kuo, V. Ozolins, and V. Yeh, Electronic structures of an epitaxial graphene monolayer on SiC(0001) after gold Intercalation: A first-principles study, *Nanotechnology* **22**, 275704 (2011).